Modelling of spatial structure of divertor footprints caused by edge-localized modes mitigated by magnetic perturbations

P Cahyna[1], M Becoulet[2], G T A Huijsmans[3], F Orain[2], J Morales[2], A Kirk[4], A J Thornton[4], S Pamela[4], R Panek[1] and M Hoelzl[5]

[1] Institute of Plasma Physics AS CR, Prague, Czech Republic

[2] CEA/IRFM, Cadarache, 13108 Saint Paul Lez Durance, France

[3] ITER Organization, Route de Vinon-sur-Verdon, CS 90 046, 13067 St. Paul Lez Durance Cedex, France

[4] CCFE, Culham Science Centre, Abingdon, Oxon, OX14 3DB, UK

[5] Max Planck Institute for Plasma Physics, Boltzmannstr. 2, 85748 Garching, Germany

Abstract. Resonant magnetic perturbations (RMPs) can mitigate the edge-localized modes (ELMs), i.e. cause a change of the ELM character towards smaller energy loss and higher frequency. During mitigation a change of the spatial structure of ELM loads on divertor was observed on DIII-D and MAST: the power is deposited predominantly in the footprint structures formed by the magnetic perturbation. In the present contribution we develop a theory explaining this effect, based on the idea that part of the ELM loss is caused by parallel transport in the homoclinic tangle formed by the magnetic perturbation of the ELM. The modified tangle resulting from the combination of the ELM perturbation and the applied RMP has the expected property of bringing open field lines in the same areas as the tangle from the RMP alone. We show that this explanation is consistent with features of the mitigated ELMs on MAST. We in addition validated our theory by an analysis of simulations of mitigated ELMs using the code JOREK. We produced detailed laminar plots of field lines on the divertor in the JOREK runs with an ELM, an applied RMP, and an ELM mitigated by the presence of the RMP. The results for an ELM clearly show a high-n rotating footprint structure appearing during the nonlinear stage of the ELM, which is not present in the early stage of the ELM. The results for a $n = 2$ RMP from the ELM control coils show the expected $n = 2$ footprint structure. The results for the mitigated ELM show a similar structure, modulated by a higher n perturbation of the ELM, consistent with our theory.

1. Introduction

Resonant magnetic perturbations (RMPs) are one of the promising methods of edge-localized mode (ELM) control in future tokamak reactors [1], which is necessary as already for ITER it is predicted that at full plasma current uncontrolled ELMs can not be tolerated [2]. The RMPs either suppress the ELMs completely or cause a change of the ELM character towards smaller energy loss and higher frequency [3]. The latter effect is called ELM mitigation and may be a viable option for ELM control on ITER if the reduction in peak heat load at the divertor is sufficient to protect the plasma-facing components. One major unknown parameter in the predictions of tolerable ELM sizes is the ELM wetted area, which together with the total ELM loss determines the peak heat load on the plasma-facing components [2, 4, 5]. The compatibility of mitigated ELMs with plasma-facing components is therefore not only determined by the ELM energy loss reduction achieved, but also by any changes of the wetted area accompanying the mitigation [4, 5]. As an example, it was observed on MAST that mitigation achieves a less significant reduction of peak ELM heat load than of the total ELM loss due to a concurrent reduction of the wetted area [6, 7]. Similar results were reported on JET with the carbon wall [8]. On the contrary on JET with the ITER-like wall the reduction of the peak heat load during ELM mitigation was partly due to an increase of the wetted area [9]. The study of spatial structure of ELM loads and its changes due to mitigation is thus important for extrapolating ELM mitigation scenarios and still an open area of research.

One significant change of the spatial structure of ELM loads on divertor during mitigation was observed on DIII-D [10], MAST [11] and NSTX [12]: the power is deposited predominantly in the footprint structures [13] formed by the magnetic perturbation. On MAST it is observed only at the early stage of the ELM, though. This effect may be one of the contributing factors to the wetted area changes. Indeed on JET footprints of heat flux are also seen during the mitigated ELM crash and were proposed as the mechanism of the wetted area increase [9]. It also can provide a valuable insight in the physics of ELMs and their mitigation. The effect suggests that the phase of the ELMs becomes locked to the phase of the applied RMP. The RMP has usually a low toroidal mode number though ($n = 2, 3$, up to $n = 4$ and 6 on MAST) while the ELM may have a higher toroidal mode number. On MAST the toroidal mode number of the ELM filaments was found to be between 10 and 20 and, remarkably, was not affected by the mitigation by $n = 4$ or $n = 6$ RMP [6]. Although a high-n ELM can nonlinearly couple to a low n perturbation [14], it is not a priori clear how this can lead to the ELM producing a structure on the divertor which corresponds to a perturbation with a much lower n.

The goal of this paper is to present a simple mechanism which may in some cases explain the observed peaking of ELM loads. It is assumed that at least a part of the ELM energy loss is caused by parallel transport along open, chaotic field lines in the homoclinic tangle formed by the magnetic component of the ELM [15]. The simplest

explanation would be thus based on the analysis of the structure of the homoclinic tangle, without considering MHD interactions of the ELMs with the applied RMP. We will show that the structure of the homoclinic tangle itself can indeed provide such an explanation. It is then needed to demonstrate that the explanation remains valid when the MHD interaction of the ELM with the RMP is taken into account. For this we will use the results of simulations of RMP-mitigated ELMs with the nonlinear MHD code JOREK. Finally we will discuss the relation of the mitigated ELM features predicted by our model to the observations on MAST.

2. Structure of the homoclinic tangle formed by the ELM and RMP

2.1. General description of the homoclinic tangle

The homoclinic tangle is formed by two intersecting surfaces — the stable and unstable invariant manifolds of the X-point [13]. The manifolds themselves are formed by field lines which approach the X-point asymptotically when followed in the direction parallel or antiparallel to the field vector. In the axisymmetric case they coincide and form the separatrix. Under the influence of the magnetic perturbation they split and their distance is in the first order approximation given by the Melnikov integral [16]. The usefulness of the concept of invariant manifolds lies in the fact that they form the boundary of the region of stochastic field lines which connect the divertor plates with the plasma core. The intersection of the stochastic region with the divertor plates manifests itself as a footprint receiving high parallel heat fluxes and having long connection length. The shape of the footprints can be calculated by tracing the connection length of field lines starting at the divertor plates and representing the result in a so-called laminar plot [17]. Alternatively the Melnikov integral can be used to approximate the shape of the manifolds. The Melnikov integral is a function of the field line label at or near the separatrix, which we call the homoclinic coordinate h [16] and define it to be equal to the toroidal angle at the outboard midplane and constant on field lines. As noted in [18], a radially displaced bundle of field lines at the outboard midplane will show up as a spiralling structure on the divertor, along a line of constant h. The displacement of the field line is caused by the magnetic perturbation and the boundary of the bundle is the invariant manifold. The Melnikov integral $M(h)$ quantifies the displacement in flux coordinate of the invariant manifold with respect to the original separatrix at the divertor plates. The shape of the footprint boundary in the $h-\psi$ space is therefore given by the equation $\psi = \max(M(h), 0)$. $M(h) < 0$ means that the manifold is inside the separatrix and therefore does not intersect the divertor. To know the footprint shape on the divertor we perform the transform from the $h - \psi$ space to the divertor coordinates $\phi - s$, where s is the radial distance along the divertor surface and ϕ the toroidal angle. The manifold will then take an elongated shape along a spiralling curve of constant h. More details can be found in [19].

The Melnikov integral can be calculated by integrating the radial component of the

perturbation along field lines on the unperturbed separatrix. For our application it is crucial that the Melnikov integral for a perturbation with a single dominant toroidal mode n will also have a simple harmonic form: $M(h) = M_n \sin(nh + h_0)$ which can be characterized only by the amplitude M_n, phase h_0 and a toroidal mode number n. There is thus very little freedom in the form of divertor footprints in a given equilibrium magnetic field. The Melnikov integral is linear: for a linear combination of perturbation fields, the resulting Melnikov integral is the corresponding linear combination of their Melnikov integrals.

## 2.2. Form of footprints of the combined ELM and RMP field

We will use the Melnikov integral formalism to calculate the footprints in the case of the ELM, in the case of the applied RMP and in the case where the ELM is present together with the RMP field, representing an mitigated ELM. We will represent here the ELM as a magnetic perturbation with a higher toroidal mode number than the RMP. For concreteness we will use $n = 8$ for the ELM and $n = 2$ for the RMP. In the $h - \psi$ space the Melnikov integrals are simple sinusoids: $M_{\mathrm{ELM}}(h) = M_{\mathrm{ELM}} \sin(8h + h_{0\mathrm{ELM}})$, $M_{\mathrm{RMP}}(h) = M_{\mathrm{RMP}} \sin(2h + h_{0\mathrm{RMP}})$. The footprints of the ELM on the divertor (with coordinates s – the radial distance along the plate and ϕ – the toroidal angle) form a similar pattern as the footprints of the RMP, only with a finer structure of spirals. Figure 1 shows the invariant manifold (red) with the curve of constant h (black, compare with fiures in [18]). Indeed, field line tracing in a simple model of the ELM magnetic perturbation indicates [18] and observations on ASDEX Upgrade confirm [20] that the ELM create a spiral-shaped heat load footprint which lies on a curve of a constant toroidal angle when mapped to the midplane (called h here), in agreement with our picture.

For the combined RMP and ELM field we start with the simplest assumption that the RMP does not have an influence on the ELM and the total field is merely a linear superposition of the RMP and a natural ELM: $M(h) = M_{\mathrm{ELM}}(h) + M_{\mathrm{RMP}}(h)$ (figure 2, left). The ELM will then act as a carrier wave modulated by the RMP and its fine footprints will be concentrated in the areas of the footprints of the RMP (figure 2, right). If we average over multiple ELMs or over time while one ELM is rotating (this can be represented by varying the phase $h_{0\mathrm{ELM}}$), the average footprint pattern of heat deposition will be similar to the one formed by the RMP alone, in agreement with experimental observations. This effect relies on the ELM perturbation amplitude to be comparable or smaller than the RMP amplitude: $M_{\mathrm{ELM}} \le M_{\mathrm{RMP}}$, otherwise the RMP structure would be obscured by the larger ELM structure.

In practice we may expect the RMP to interact with the ELM, in particular to decrease its amplitude (mitigation). This does not significantly affect our reasoning and may help to satisfy the relation $M_{\mathrm{ELM}} \le M_{\mathrm{RMP}}$ even in cases where it is not satisfied for unmitigated ELMs.
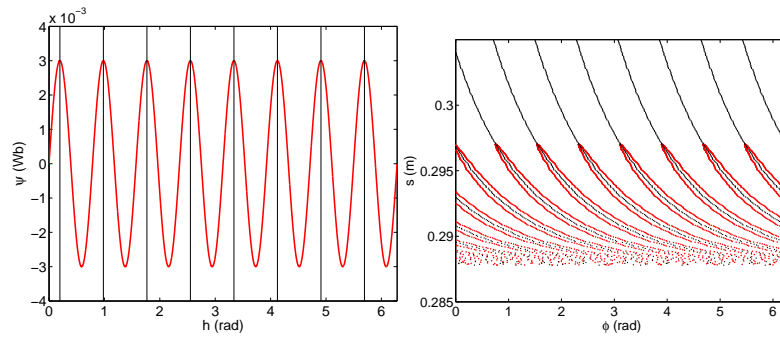
Figure 1. Footprints of a $n = 8$ ELM in the in the $h - \psi$ coordinates (left) and divertor coordinates (right). Black curves: coordinate curves of constant h.
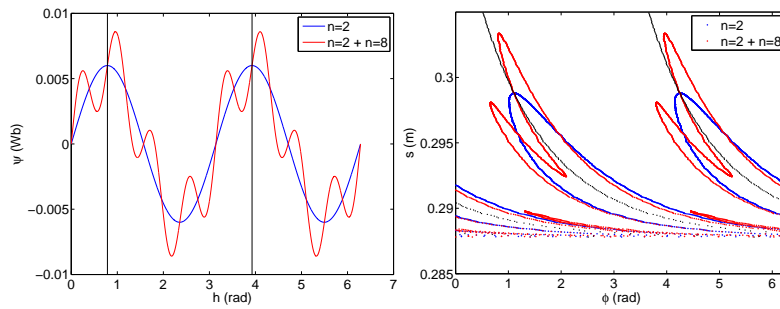

Figure 2. Footprints of a $n = 2$ RMP (blue) and superposed with a $n = 8$ ELM (red) in the $h - \psi$ coordinates (left) and the divertor coordinates (right).

3. Verification of the model using MHD simulations

3.1. Form of footprints in the MHD simulations

In the previous sections we developed an understanding of the form of mitigated ELM divertor footprints based on a very simple representation of the perturbed magnetic field. We shall now verify the model in a more realistic magnetic field and a full 3-D geometry. Such calculations were already performed in [21] where the ELM field was modelled using a source formed of a set of equidistant current filaments. Here we will use an even more realistic model: MHD simulations of the ELM crash with the code JOREK [22, 23], including RMPs. The simulations were run for a JET-like equilibrium. The JOREK simulations use a Fourier representation in the toroidal direction, harmonics $n = 0, 2, 4, 6, 8$ were used in the present simulations. The applied RMP is here produced by the error field correction coils (EFCCs) of JET, but only the dominant $n = 2$ toroidal harmonic of their field is present (as the boundary condition for the $n = 2$ toroidal harmonic of the simulated field), the higher n sidebands that occur in realistic coil designs are omitted for simplicity. More details on the simulations can be found in [24, 25]. The evolutions of magnetic energies of the toroidal modes are shown in figure 3, together with the time instants where the following figures are taken.
  figure 4 shows laminar plots on the divertor calculated for three time instants during
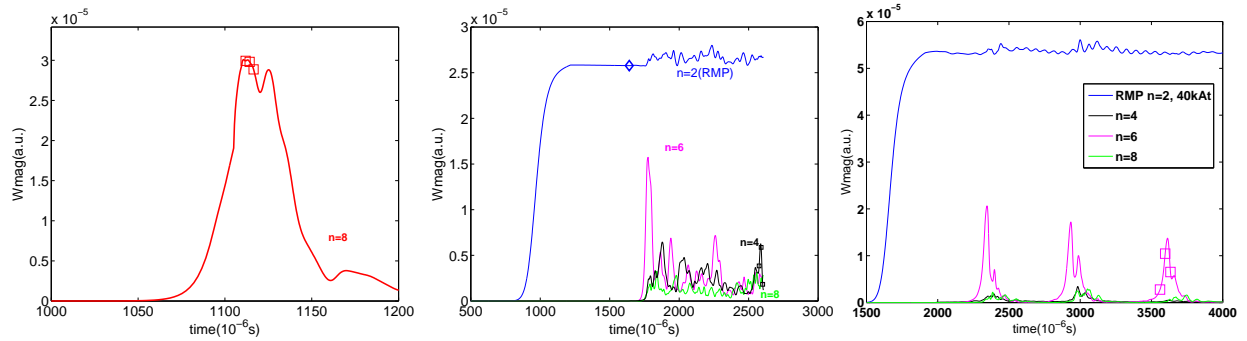
Figure 3. Time evolution of the magnetic energies of the modes in the JOREK simulations used: ELM crash without RMP (left, corresponding to figure 4), $n = 2$ RMP and mitigated ELMs (center, corresponding to figure 5) and ELM cycles not mitigated by RMP (right, corresponding to figure 6). The symbols show the time instants corresponding to the following laminar plots.
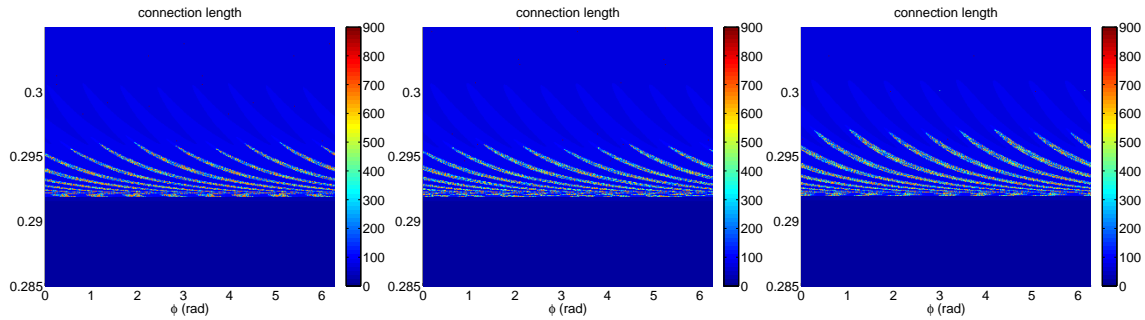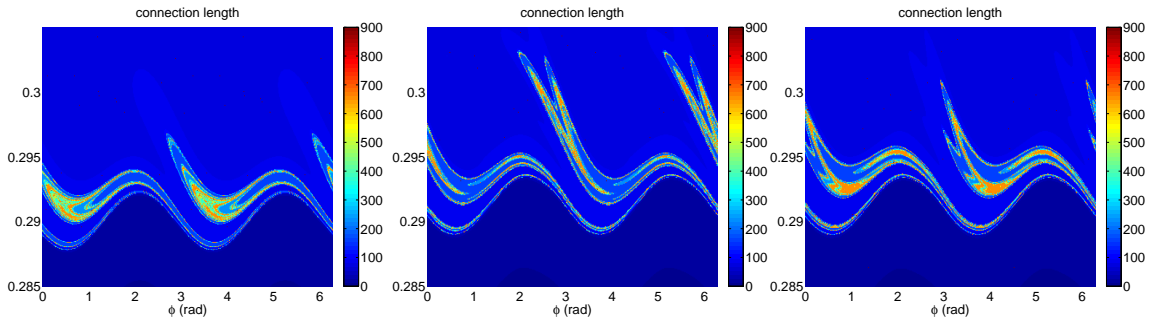

Figure 4. Connection length on divertor during an ELM crash modelled by JOREK in three time instants: $1.1119 \cdot 10^{-3}$ s, $1.1142 \cdot 10^{-3}$ s, $1.1165 \cdot 10^{-3}$ s.

the ELM crash in a JOREK simulation. The dominant toroidal mode number is $n = 8$ here, corresponding to the 8 visible footprint lobes. We may see that the whole pattern is rotating.

The next simulations were run with a $n = 2$ RMP similar to the one produced by JET EFCCs. Figure 5 shows the resulting laminar plot without ELMs (produced by running the simulation with $n = 0$ and $n = 2$ harmonics only) and with an ELM crash (using the harmonics $n = 0 \ldots 8$ with a step of 2). The primary strike point is distorted into an undulating pattern due to the perturbation being non-negligible in the X-point area. The footprint pattern with an ELM shows a similar $n = 2$ structure as without an ELM on a large scale, but its boundary has a more complex shape with multiple spirals on a smaller scale. The fine scale structures evolve over time while the large scale $n = 2$ footprints remain mostly the same.

It should be noted that while without the RMP the dominant toroidal mode number of the ELMs is $n = 8$, with the RMP the energy "cascades" to lower modes $n = 4, 6$ due to their nonlinear coupling [14] as detailed in [25]. We are also interested in cases where the toroidal mode number is unchanged by the RMP, corresponding to the experimental observations on MAST. Such a case is provided by a JOREK simulation

Figure 5. Connection length on divertor with a $n = 2$ RMP (left) and together with an ELM crash in two time instants (center: $t = 2.576 \cdot 10^{-3}$ s; right: $t = 2.601 \cdot 10^{-3}$ s).

with an increased diamagnetic rotation, where the $n = 6$ mode is the most unstable and is not mitigated by RMP corresponding to a current of 40 kAt in the EFCCs [24]. The results for three time instants are shown in figure 6. The laminar plot has a $n = 2$ pattern, split into a structure of finer footprints which evolve over time while conserving the basic $n = 2$ pattern.
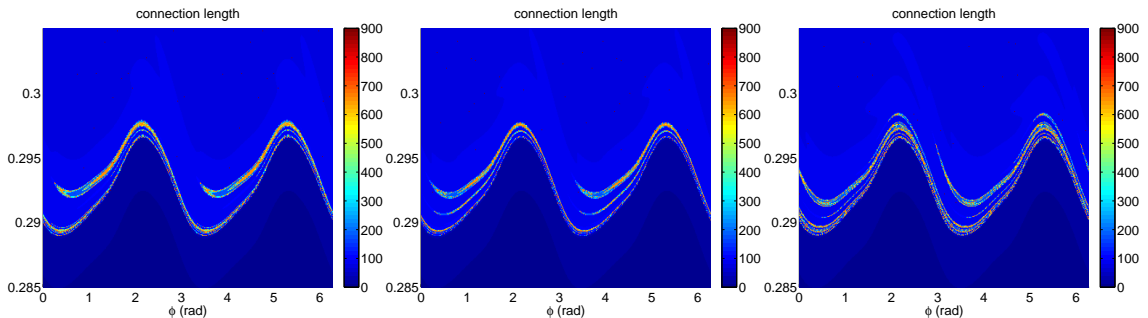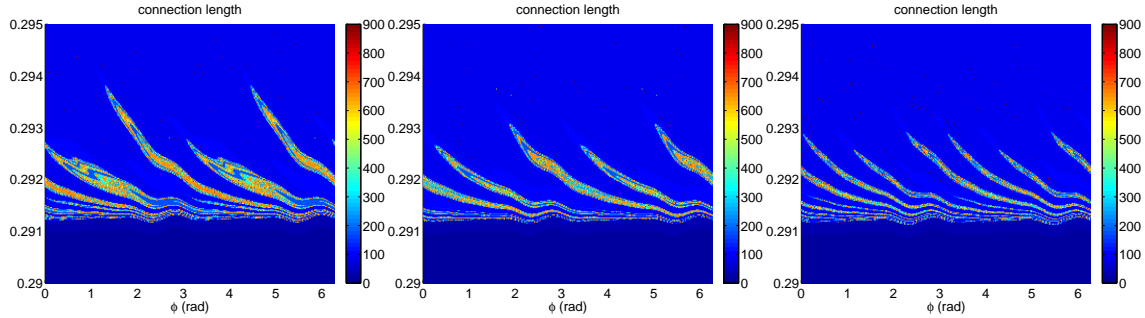

Figure 6. Connection length on divertor with a $n = 2$ RMP and an ELM crash with a dominant $n = 6$ mode in three time instants: $3.5599 \cdot 10^{-3}$ s, $3.5966 \cdot 10^{-3}$ s, $3.6332 \cdot 10^{-3}$ s.

3.2. Footprint rotation

We may observe that without the magnetic perturbation the footprints rotate in the direction of the increasing toroidal angle ϕ. This is the clockwise direction when viewed from top and is also the direction of the electron diamagnetic and $E \times B$ drifts, in which the ballooning instability rotates [26]. With the magnetic perturbation, the fine details of the boundary fluctuate, which may be due to the rotation of the higher n modes due to the ELMs. The superposition with the dominant $n = 2$ pattern from the RMP does not allow to distinguish the rotation clearly, though. For this reason we performed the field line tracing again in a field constructed by subtracting the $n = 2$ mode from the total field, while the higher modes are being kept. The $n = 2$ mode is still present in the MHD simulation and thus modifies the other modes via nonlinear coupling, it is removed only in the field line tracing step. The footprints calculated in this way are

somewhat artificial — they do not correspond to power loads on the divertor in any way — but allow us to determine the rotation of the higher modes (corresponding to ELMs). The laminar plots corresponding to figure 5 (with one plot added at an intermediate time instant) are shown in figure 7. The footprint pattern still rotates in the direction

Figure 7. Connection length on divertor with a mitigated ELM, using only $n = 0, 4, 6, 8$ components of the magnetic field, in three time instants (left: $t = 2.576 \cdot 10^{-3}$ s; center: $t = 2.590 \cdot 10^{-3}$ s, right: $t = 2.601 \cdot 10^{-3}$ s).

of increasing ϕ, albeit more slowly than in the unmitigated phase. Due to the presence of multiple modes, the pattern does not only rotate, but also progressively changes its shape as the relative amplitudes of the modes vary. We may also note that the periodic distortion of the primary strike point due to the RMP has vanished. For comparison, figure 7 shows the poloidal profiles of density at the same time instants (in this case with all the harmonics including $n = 2$). The pattern rotates in the electron diamagnetic direction (counterclockwise).
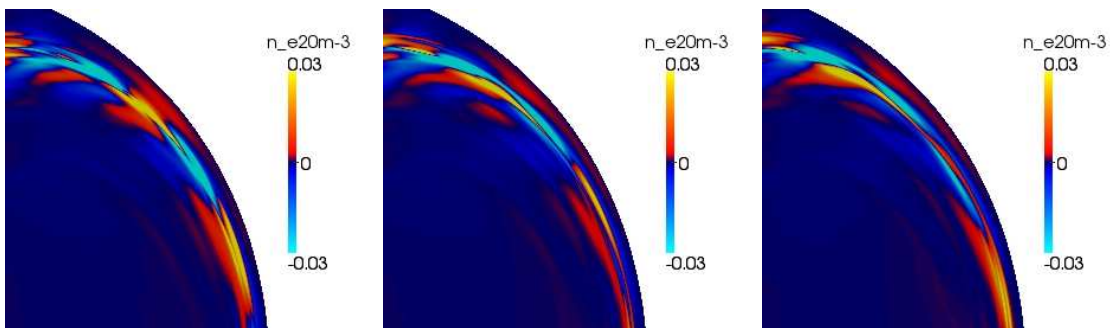
Figure 8. Density in the poloidal plane during the mitigated ELM crash in three time instants (left: $t = 2.576 \cdot 10^{-3}$ s; center: $t = 2.590 \cdot 10^{-3}$ s, right: $t = 2.601 \cdot 10^{-3}$ s).

For the case when the RMP does not mitigate the ELMs (figure 6) the corresponding laminar plot without the $n = 2$ mode is shown in figure 9. Again, the footprint pattern of the ELM rotates and changes its shape.
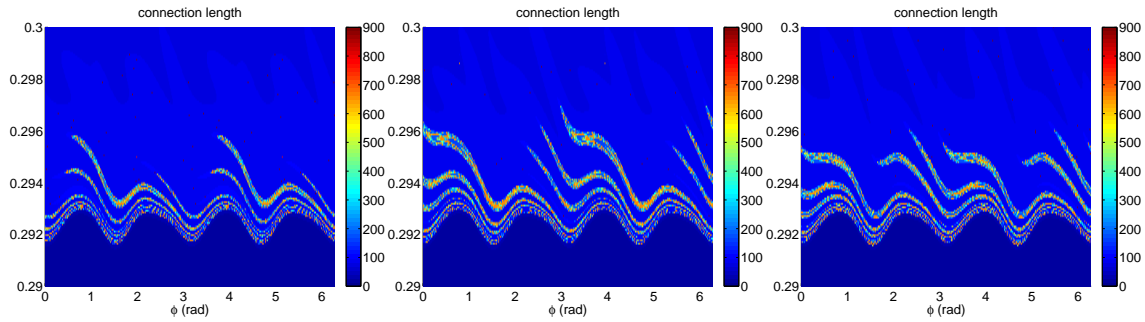
Figure 9. Connection length on divertor with a $n = 2$ RMP and an ELM crash with a dominant $n = 6$ mode, using only $n = 0, 4, 6, 8$ components of the magnetic field, in three time instants: $3.5599 \cdot 10^{-3}$ s, $3.5966 \cdot 10^{-3}$ s, $3.6332 \cdot 10^{-3}$ s.

4. Discussion and conclusion

We have shown that a simple linear superposition of the field of an ELM and an applied RMP field leads to concentration of open field lines in the footprints of the RMP field. (Remarkably, our model does not rely on any nonlinear interaction between the ELM and the RMP, although such an interaction is known to occur in the MHD simulations [25, 14].) Assuming that at least a part of the ELM loss is caused by parallel transport along field lines, this would lead to an apparent "locking" of the divertor heat flux pattern to the RMP even though the ELM has a different toroidal mode number and its rotation may not actually lock. This was indeed observed on MAST, where though the ELM heat flux follows the RMP footprints only when averaged over the start of the ELM pulse. This result can be reconciled with our model by using the fact that a part of the ELM energy is carried away by filaments and only the rest may be caused by the transport in the homoclinic tangle assumed here. Furthermore, the filaments arrive at the target with a delay [27]. If the structure of the filament losses is unaffected by the RMP, they will in a later stage of the ELM crash blur the pattern caused by the stochastic transport in the beginning, explaining the observed effect. We shall note that only the structure of the stochastic losses was studied here and further research is needed to determine if the RMP has any impact on the filament losses or not. We also studied only the connection length in the JOREK simulations, as a too high perpendicular diffusion needed for numerical stability reasons prevented us from extracting meaningful target power profiles. Solving this problem will allow us to tackle also the filament question.

While our theory predicts that the footprints will have generally the shape of the RMP footprints, the ELM field causes an additional distortion of their edge, depending on the relative amplitude of the ELM compared to the RMP. If the footprints due to the ELM field are longer than those due to the RMP, the RMP structure may even stop being distinguishable. This may explain the NSTX results where the RMP structure was seen only in smaller ELMs [12], assuming that larger ELMs have longer footprints. The distortion of the footprints was seen especially in the $n = 6$ JOREK runs, where the

ELMs are not mitigated. This fine distortion is moving across the static RMP pattern in the JOREK simulations. The modification of the static RMP pattern was proposed in [21] as the explanation of MAST results where the ELM load follows the footprints only in some ELMs. If the phase of the ELM is such that its Melnikov integral has a constructive interference with the one of the RMP at the footprint tip, the footprint will become longer and thus better observable. On the other hand, a destructive interference at the tip will reduce it. In [21] it was noted that this explanation requires that the ELM phase locks (i. e., does not rotate). This is a different regime than observed in the JOREK results where the phase always rotates. The rotation was observed to slow down though in our simulations, so if the change of phase is negligible during the infra-red camera exposure time (35 μs on MAST), the result may be indistinguishable from complete locking of the phase. In this way the experimental observations may be reconciled with the simulations.

Our model relies only on the general assumption that an ELM has a magnetic component which can form a homoclinic tangle, and does not depend on a particular origin of this field. We have seen that JOREK simulations predict the existence of such a field during the ELM crash. Another suggestion was that such a field is generated by thermoelectric currents flowing through the homoclinic tangle [28]. We may say that this theory is not needed for a qualitative explanation of the experimental results, as JOREK simulations do not include the thermoelectric currents and still show the effect. It may be the case though that a quantitative analysis will show the need for the thermoelectric currents in order to explain the data. Such a claim was made in [29], where it was found that the vacuum RMP footprints do not match those observed during the mitigated ELMs on JET. The model used in [29] did not apparently include the field of the ELM itself, so the possibility that the vacuum RMP field superposed with the ELM field will be sufficient to match the data can not be completely ruled out yet.

Further work shall concentrate on determining the changes of the ELM wetted area due to the effect described here. An increase of the wetted area due to RMPs was reported [9] on JET with the ITER-like wall (contrary to the carbon wall results) and attributed to the observed footprint pattern, while on MAST the wetted area was found to decrease [6, 7, 11]. The latter effect is probably not due to the footprint pattern, as it follows the same scaling as the unmitigated ELMs. Other possible mechanisms behind the footprint pattern in mitigated ELMs should be investigated. For instance, if an ELM has a toroidal mode number equal to the one of the RMP, it may directly lock to it, as suggested in [10], and produce a large pattern due to constructive interference. The influence of RMPs on the filament pattern shall be modeled, as filaments are responsible at least for a part of the ELM loss.

Acknowledgments

References

[1] T.E. Evans. ELM mitigation techniques. *Journal of Nuclear Materials*, 438, Supplement:S11 – S18, 2013.

[2] A. Loarte, G. Huijsmans, S. Futatani, L.R. Baylor, T.E. Evans, D. M. Orlov, O. Schmitz, M. Becoulet, P. Cahyna, Y. Gribov, A. Kavin, A. Sashala Naik, D.J. Campbell, T. Casper, E. Daly, H. Frerichs, A. Kischner, R. Laengner, S. Lisgo, R.A. Pitts, G. Saibene, and A. Wingen. Progress on the application of ELM control schemes to ITER scenarios from the non-active phase to DT operation. *Nuclear Fusion*, 54(3):033007, 2014.

[3] M.E. Fenstermacher. Elm control by resonant magnetic perturbations: Overview of research by the ITPA pedestal and edge physics group. In *IAEA Fusion Energy Conference 2010 (Proc. 23rd IAEA FEC Daejeon, 2010)*, pages ITR/P1–30, (Vienna: IAEA), 2012.

[4] H. Thomsen, T. Eich, S. Devaux, G. Arnoux, S. Brezinsek, E. delaLuna, W. Fundamenski, A. Herrmann, A. Huber, S. Jachmich, P. Lomas, I. Nunes, G. Saibene, A. Scarabosio, J. Schweinzer, and JET EFDA Contributors. Power load characterization for type-I ELMy H-modes in JET. *Nuclear Fusion*, 51(12):123001, 2011.

[5] T. Eich, H. Thomsen, W. Fundamenski, G. Arnoux, S. Brezinsek, S. Devaux, A. Herrmann, S. Jachmich, and J. Rapp. Type-I ELM power deposition profile width and temporal shape in JET. *Journal of Nuclear Materials*, 415(1, Supplement):S856 – S859, 2011. Proceedings of the 19th International Conference on Plasma-Surface Interactions in Controlled Fusion.

[6] A Kirk, I T Chapman, J Harrison, Yueqiang Liu, E Nardon, S Saarelma, R Scannell, A J Thornton, and the MAST team. Effect of resonant magnetic perturbations with toroidal mode numbers of 4 and 6 on edge-localized modes in single null H-mode plasmas in MAST. *Plasma Physics and Controlled Fusion*, 55(1):015006, 2013.

[7] A Kirk, Yueqiang Liu, I T Chapman, J Harrison, E Nardon, R Scannell, A J Thornton, and the MAST Team. Effect of resonant magnetic perturbations on ELMs in connected double null plasmas in MAST. *Plasma Physics and Controlled Fusion*, 55(4):045007, 2013.

[8] S. Jachmich, G. Arnoux, S. Brezinsek, S. Devaux, T. Eich, W. Fundamenski, C. Giroud, H.R. Koslowski, Y. Liang, E. de la Luna, G. Maddison, and H. Thomsen. Power and particle fluxes to plasma-facing components in mitigated-ELM h-mode discharges on JET. *Journal of Nuclear Materials*, 415(1, Supplement):S894 – S900, 2011. Proceedings of the 19th International Conference on Plasma-Surface Interactions in Controlled Fusion.

[9] Y. Liang, P. Lomas, I. Nunes, M. Gryaznevich, M.N.A. Beurskens, S. Brezinsek, J.W. Coenen, P. Denner, Th. Eich, L. Frassinetti, S. Gerasimov, D. Harting, S. Jachmich, A. Meigs, J. Pearson, M. Rack, S. Saarelma, B. Sieglin, Y. Yang, L. Zeng, and JET-EFDA Contributors. Mitigation of type-I ELMs with n=2 fields on JET with ITER-like wall. *Nuclear Fusion*, 53(7):073036, 2013.

[10] M.W. Jakubowski, T.E. Evans, M.E. Fenstermacher, M. Groth, C.J. Lasnier, A.W. Leonard, O. Schmitz, J.G. Watkins, T. Eich, W. Fundamenski, R.A. Moyer, R.C. Wolf, L.B. Baylor, J.A. Boedo, K.H. Burrell, H. Frerichs, J.S. deGrassie, P. Gohil, I. Joseph, S. Mordijck, M. Lehnen,

C.C. Petty, R.I. Pinsker, D. Reiter, T.L. Rhodes, U. Samm, M.J. Schaffer, P.B. Snyder, H. Stoschus, T. Osborne, B. Unterberg, E. Unterberg, and W.P. West. Overview of the results on divertor heat loads in RMP controlled H-mode plasmas on DIII-D. *Nuclear Fusion*, 49(9):095013, 2009.

[11] A.J. Thornton, A. Kirk, I.T. Chapman, and J.R. Harrison. Divertor heat fluxes and profiles during mitigated and unmitigated edge localised modes (ELMs) on the mega amp spherical tokamak (MAST). *Journal of Nuclear Materials*, 438, Supplement(0):S199 – S202, 2013. Proceedings of the 20th International Conference on Plasma-Surface Interactions in Controlled Fusion Devices.

[12] J-W Ahn, F Scotti, K Kim, J M Canik, J D Lore, R Maingi, A G McLean, R E Bell, A Diallo, S P Gerhardt, T K Gray, S M Kaye, B P LeBlanc, V A Soukhanovskii, and K Tritz. Characterization of divertor footprints and the pedestal plasmas in the presence of applied n=3 fields for the attached and detached conditions in NSTX. *Plasma Physics and Controlled Fusion*, 56(1):015005, 2014.

[13] T E Evans, R K W Roeder, J A Carter, B I Rapoport, M E Fenstermacher, and C J Lasnier. Experimental signatures of homoclinic tangles in poloidally diverted tokamaks. *Journal of Physics: Conference Series*, 7:174–190, 2005.

[14] I. Krebs, M. Hoelzl, K. Lackner, and S. Guenter. Nonlinear excitation of low-n harmonics in reduced magnetohydrodynamic simulations of edge-localized modes. *Physics of Plasmas*, 20(8):082506, 2013.

[15] G.T.A. Huijsmans and A. Loarte. Non-linear MHD simulation of ELM energy deposition. *Journal of Nuclear Materials*, 438, Supplement(0):S57 – S63, 2013. Proceedings of the 20th International Conference on Plasma-Surface Interactions in Controlled Fusion Devices.

[16] S. Wiggins. *Introduction to applied nonlinear systems and chaos.* Number 2 in Texts in Applied Mathematics. Springer-Verlag, New York Berlin Heidelberg, 1996.

[17] A. Wingen, T. E. Evans, and K. H. Spatschek. Footprint structures due to resonant magnetic perturbations in DIII-D. *Physics of Plasmas*, 16(4):042504, 2009.

[18] T. Eich, A. Herrmann, and J. Neuhauser. Nonaxisymmetric energy deposition pattern on ASDEX Upgrade divertor target plates during type-I edge-localized modes. *Phys. Rev. Lett.*, 91:195003, Nov 2003.

[19] P. Cahyna, M. Peterka, E. Nardon, H. Frerichs, and R. Panek. Method for comparison of tokamak divertor strike point data with magnetic perturbation models. *Nuclear Fusion*, 54(6):064002, 2014.

[20] T Eich, A Herrmann, J Neuhauser, R Dux, J C Fuchs, S Gãijnter, L D Horton, A Kallenbach, P T Lang, C F Maggi, M Maraschek, V Rohde, W Schneider, and the ASDEX Upgrade Team. Type-I ELM substructure on the divertor target plates in ASDEX Upgrade. *Plasma Physics and Controlled Fusion*, 47(6):815, 2005.

[21] A.J. Thornton, A. Kirk, P. Cahyna, I.T. Chapman, J.R. Harrison, Yueqiang Liu, and the MAST Team. The effect of resonant magnetic perturbations on the divertor heat and particle fluxes in MAST. *Nuclear Fusion*, 54(6):064011, 2014.

[22] G T A Huysmans, S Pamela, E van der Plas, and P Ramet. Non-linear MHD simulations of edge localized modes (ELMs). *Plasma Physics and Controlled Fusion*, 51(12):124012, 2009.

[23] F. Orain, M. Becoulet, G. Dif-Pradalier, G. Huijsmans, S. Pamela, E. Nardon, C. Passeron, G. Latu, V. Grandgirard, A. Fil, A. Ratnani, I. Chapman, A. Kirk, A. Thornton, M. Hoelzl, and P. Cahyna. Non-linear magnetohydrodynamic modeling of plasma response to resonant magnetic perturbations. *Physics of Plasmas*, 20(10), 2013.

[24] M. Becoulet, F. Orain, J. Morales, X. Garbet, G. Dif-Pradalier, C. Passeron, G. Latu, E. Nardon, A. Fil, and V. Grandgirard. Non-linear MHD modelling of edge localized modes and their interaction with resonant magnetic perturbations in rotating plasmas. In *IAEA Fusion Energy Conference 2014 (Proc. 25th IAEA FEC Saint-Petersburg, 2014)*, pages TH/6–1Rb, (Vienna: IAEA), 2015.

[25] M. Bécoulet, F. Orain, G. T. A. Huijsmans, S. Pamela, P. Cahyna, M. Hoelzl, X. Garbet, E. Franck,

E. Sonnendrücker, G. Dif-Pradalier, C. Passeron, G. Latu, J. Morales, E. Nardon, A. Fil, B. Nkonga, A. Ratnani, and V. Grandgirard. Mechanism of edge localized mode mitigation by resonant magnetic perturbations. *Phys. Rev. Lett.*, 113:115001, Sep 2014.

[26] J.A. Morales, M. Bécoulet, F. Orain, X. Garbet, G. Dif-Pradalier, C. Passeron, and G.T.A. Huijsmans. Rotation of edge localized modes and their filaments. In *Proceedings of the 41st EPS Conference on Plasma Physics*, volume 38F of *Europhysics Conference Abstracts*, page P1.063, 2014.

[27] A Kirk, G F Counsell, G Cunningham, J Dowling, M Dunstan, H Meyer, M Price, S Saarelma, R Scannell, M Walsh, H R Wilson, and the MAST team. Evolution of the pedestal on MAST and the implications for ELM power loadings. *Plasma Physics and Controlled Fusion*, 49(8):1259, 2007.

[28] A. Wingen, T. E. Evans, C. J. Lasnier, and K. H. Spatschek. Numerical modeling of edge-localized-mode filaments on divertor plates based on thermoelectric currents. *Phys. Rev. Lett.*, 104:175001, Apr 2010.

[29] M. Rack, B. Sieglin, J. Pearson, T. Eich, Y. Liang, P. Denner, A. Wingen, L. Zeng, I. Balboa, S. Jachmich, and JET-EFDA Contributors. Modified heat load deposition of the ELM crash due to n=2 perturbation fields at JET. *Nuclear Fusion*, 54(6):064012, 2014.